AIAA JOURNAL
Vol. 39, No. 8, August 2001

Mixing Effects Between Self-Sustained and Unstable Hydrodynamic Oscillations Near Injecting Walls

Jérôme Vétel,* Frédéric Plourde,† and Son Doan-Kim‡
Ecole Nationale Superieure Mécanique et d'Aerotechnique, 86960 Futuroscope, France

Self-sustained oscillations in a shear layer were studied in a confined chamber with injecting walls. Experiments were carried out over a wide range of Reynolds numbers ($0.86 \times 10^5 \le Re \le 1.94 \times 10^5$) and of Mach numbers ($0.05 \le M \le 0.227$) in order to underline the effect of dynamic conditions on the pressure amplifications and on the excited acoustic modes. The presence of an obstacle generated a highly sheared flow in which vortex-shedding frequency was set by an acoustic-hydrodynamic coupling. The Mach number controlled the selectivity process of the vortex-shedding frequency, but turbulence dissipation weakened this coupling by a loss of structure coherence. As this did not affect the pressure fluctuation level, a second noise source was detected; vortices near the injecting wall, resulting from a mixing effect between shear-layer oscillations and injection flow through the porous wall, were identified. This latter was found to have a sensible influence on the self-sustained oscillations in such segmented flows.

Nomenclature

$A(\tau)$	=	envelope signal of $R_{u'P'}(\tau)$ (dimensionless parameter)
a	=	sound velocity, m/s, $\sqrt{(\gamma r T)}$
d_1, d_2, d_3, d_4	=	characteristic length, m
f_{nL}	=	nth longitudinal acoustic mode, Hz, $na/2L$
h_c	=	channel height, m
h_t	=	height of the nozzle throat, m
It	=	turbulence intensity, $\sqrt{(\overline{u'^2} + \overline{v'^2})}/u_v$
$It_{\max}$	=	maximum turbulence intensity at fixed X profile
L	=	channel length, m
l	=	distance between the obstacle location and the nozzle location
M	=	Mach number (dimensionless parameter), u_v/a
M_0	=	Mach-number threshold (dimensionless parameter)
P	=	mean pressure at the front head, Pa
P'	=	fluctuating pressure, Pa
q_m	=	mass flow rate, kg/s
Re	=	Reynolds number (dimensionless parameter), $\rho u_v h_c/\mu$
$R_{u'P'}(\tau)$	=	correlation coefficient of pressure and velocity fluctuations (dimensionless parameter), $\overline{u'(t) \cdot P'(t+\tau)}/\sqrt{[u'(t)^2]} \cdot \sqrt{[P'(t)^2]}$
$R_{u_1u_2}(\tau, \delta_x, \delta_y)$	=	correlation coefficient of u_1 and u_2 velocity fluctuations (dimensionless parameter), $\overline{u'_1(t) \cdot u'_2(t+\tau)}/\sqrt{(u'^2_1)}\sqrt{(u'^2_2)}$
Sr	=	Strouhal number (dimensionless parameter)
s	=	characteristics surface area, m^2, wh_c
T	=	temperature of the flow, K
u, v	=	velocity components respectively in X, Y direction, m/s
u_c	=	coherent structure velocity, m/s
u_v	=	characteristic velocity based on the mass flow rate, m/s, $q_m/\rho s$
u', v'	=	characteristic fluctuation velocity components in X, Y direction, m/s
$\overline{u'v'}$	=	turbulence shear stress, m^2/s^2
w	=	channel width, m
X, Y, Z	=	nondimensional axis normalized respectively by l, h_c, and w
X_c	=	nondimensional critical location
γ	=	specific heat ratio (dimensionless parameter)
δ_x	=	distance in X direction between two probes, m
δ_y	=	distance in Y direction between two probes, m
μ	=	dynamic viscosity, kg/ms
ρ	=	density, kg/m^3
σ_v	=	pseudo-injected turbulence ratio (dimensionless parameter)
τ	=	time delay, s

I. Introduction

HYDRODYNAMICS and acoustics coupling can be one of the most serious phenomena capable of generating and developing dangerous instabilities in solid propellant rocket motors. Different studies[1–3] have reported on the presence of pressure and thrust oscillations in such motors. The presence of a sheared flow in a confined chamber can create a high potential for unstable behavior. First, motors may be acoustically assimilated to a closed-closed chamber favoring acoustic mode excitation while the chamber acts as a resonator. At that time geometry is mainly characterized by a higher length-diameter ratio favoring low acoustic frequencies and by some other constraints. For instance, segmentation of the propellant blocks introduces sheared areas in burnt gas flow either in the discontinuities between propellant blocks or through the emergence of thermal protections. As underlined by Vuillot,[4] classical stability calculations based on the conventional acoustic balance[5] fail in the description of solid propellant rocket motor behavior, and this difference can be explained by attributing such oscillations to a periodic vortex-shedding phenomenon. Acoustic mode excitation is linked to hydrodynamic vortex instabilities, which are the source of acoustic energy. The amplification of these acoustic waves reaches a maximum level when the characteristic vortex-shedding frequency is close to a natural frequency of the chamber. Under these conditions a feedback phenomenon may occur as a form of interaction between aerodynamics and acoustics. This coupling was well identified in cold gas facilities by simulating flow development in the chamber. Dunlap and Brown[6] demonstrated the presence of the periodic vortex phenomenon, as did Plourde et al.[7] and Avalon.[8] In fact, Avalon demonstrated the presence of vortices in a walled porous channel in which no restrictor was present. The interaction of the main flow

Received 30 March 2000; revision received 8 December 2000; accepted for publication 15 December 2000.

*Mechanical Engineer, Laboratoire d'Etudes Thermique, Téléport 2, 1 Avenue Clément Ader, BP 109.
†CNRS Researcher, Laboratoire d'Etudes Thermique, Téléport 2, 1 Avenue Clément Ader, BP 109.
‡Professor, Laboratoire d'Etudes Thermique, Téléport 2, 1 Avenue Clément Ader, BP 109.

and the injected flow at the wall sufficed to create vortices above the injected wall generating sufficient noise. Even if the interaction between the sheared flow and acoustics have been well identified, our comprehension of such instabilities remains to be enhanced. Furthermore, since today's tendency is to develop well-adapted control of stability in such engines,[9] it is necessary to develop our basic knowledge of this coupling and its sensitivity to either the dynamic conditions of the flow or to the nature of the flow itself. The aim of our study is to simulate by means of a cold gas facility the internal behavior of a solid rocket motor of Ariane 5's launcher and to analyze the unstable behavior of the flow with regard to the Mach number and the Reynolds number.

II. Experimental Setup and Measuring Techniques

A. Test Channel

The experimental apparatus is a $\frac{1}{40}$ scale model of the solid propellant booster of Ariane 5. As depicted in previous works,[7,10,11] the scale model did not completely reproduce the actual full-scale motor, but the latter was roughly similar through the presence of segmented blocks, wall injection, and submerged nozzle. In terms of internal design, the test channel was a 0.050-m-wide, nonsymmetric, two-dimensional channel. All other dimensions are given in Fig. 1. As depicted in this figure, three segmented injecting blocks were located in the chamber and between each block; an obstacle emerged above the porous walls, which restricted by 32% the passage through the channel. The first injecting block represented the ignition propellant block of the full-scale motor. As the latter burnt rapidly, the first block was not fed with air. Thus, we focused our study on the second obstacle and within its wake. Combustion simulation was performed by injecting air at ambient temperature issuing from a feeding unit whose mass flow rate could vary from 0.050 to 0.300 kg/s. Injection into the channel was carried out through a porous wall mainly characterized by a sintered-bronze sphere Poral plat with 2-μm characteristic diameter and a flexible metallic weaved sieve set at 10 mm above the Poral plate. The uniformity of the mass flow rate distribution along the porous wall was controlled by an accurate feeding system. In fact, airflow was fed into a general manifold and was divided into 20 flexible polyamide tubes. Each tube fed in its turn an isolated cell, and the mass flow rate in each injection cell was controlled by sonic air inlets. The role of each isolated cell was to feed a given Poral plate area. The assumption of an uniformity was verified previously in computing the change of the mean velocity all along the chamber.[10] Its linear change demonstrated the uniformity of the injection in our test channel. The Poral plate enabled us to isolate the flow in the chamber while the metallic weaved sieve significantly reduced the injected turbulence in the chamber. Beddini[12] conducted numerical investigations in which the pseudo-injected turbulence ratio $\sigma_v = \sqrt{v'^2}/v$ was found to be one of the most important parameters in the flowfield calculation. Because of a metallic weaved sieve, it allowed us to significantly decrease σ_v from 10% to a level lower than 4% and then to control the injecting boundary conditions. A nozzle with sonic throat was located at the rear end of the chamber to ensure the acoustic isolation of the channel from exterior environment. The height of the nozzle throat h_t could be varied, thereby allowing for the mean pressure P and M control. The simulation principle was based on the similarity with the actual size motor by conserving the Mach and Strouhal numbers. In fact, the frequency of oscillations is typically expressed by the Strouhal number. We considered the global Strouhal number $Sr = fl/u$, in which l is the length between

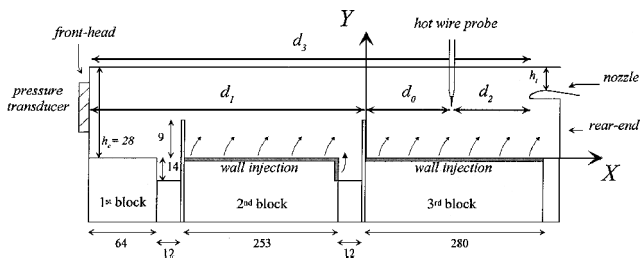

Fig. 1 Experimental configuration. All sizes are in millimeters.

Table 1 Experimental conditions[a]

q_m (10^{-3} kg/s)	Re (10^5)	h_t (10^{-3} m)	P (10^5 Pa)	M
80	0.86	2.20–4.73	1.45–3.00	0.050–0.098
89	0.96	2.98–5.48	1.42–2.57	0.061–0.112
105	1.14	3.05–6.45	1.40–2.91	0.063–0.133
119	1.29	3.37–7.29	1.40–2.95	0.070–0.151
134	1.45	4.09–8.08	1.42–2.73	0.084–0.167
150	1.62	4.47–9.47	1.41–2.92	0.092–0.195
179	1.94	5.26–10.97	1.41–2.82	0.110–0.227

[a]Air temperature, 298 K; acoustic mode f_{1L}, 278 Hz; acoustic mode f_{2L}, 556 Hz; and hydrodynamic critical location X_c 1.58.

separation and impingement. Assuming a potential vortex-shedding phenomenon in the wake of the obstacle, l was taken as the length between the location of the obstacle and the submerged nozzle location. f was the first longitudinal acoustic mode, and u was equal to the u_v characteristic velocity in the chamber. Because of a Strouhal- and Mach-number simulation, the Reynolds-number range of our experiments was an order of magnitude smaller than that found in the full-scale motor. We stated this point in Sec. V. Focusing our study on the effect of hydrodynamic conditions, one of the main parameter was the Reynolds number that can be expressed as a direct function of the injected mass flow rate:

$$Re = \rho u_v h_c/\mu = q_m/w\mu \tag{1}$$

Furthermore, internal velocity was also considered as an important parameter. Assuming a constant injected mass flow rate, i.e., a fixed Reynolds number, the nozzle throat was progressively closed or opened by stages at intervals of 0.05 mm. The mass flow rate balance between the channel section and the nozzle throat section can be estimated through the link between h_t and M:

$$M = \sqrt{(2/\gamma + 1)^{\gamma+1/\gamma-1}}\, h_t/h_c \tag{2}$$

In fact, Eq. (2) is a very accurate expression for low-Mach-number evaluation. Furthermore, all of the experiments presented in this paper were obtained with a choked nozzle. The complete details of experimental conditions are given in Table 1.

B. Measurement Techniques

Various measuring techniques were employed. Mean pressure and its fluctuating component measurements were obtained at the head end with a 7261 Kistler piezo-electric quartz transducer, whose sensitivity was about 10 Pa. This transducer allows one to adapt the transducer via a flush mounting at the head end. Acquisition and analysis of the data (more than 200,000 samples) at 10-kHz frequency made it possible to determine the mean pressure level, the standard deviation, and the spectral content in the pressure field. Spectral analysis decomposition was performed with blocks of 4096 data with 2.44-Hz frequency resolution and a spectral accuracy of about 5%. The same control was applied to the velocity signals, measured by a Dantec 5-μm single miniature probe and with a 5-μm X miniature probe. The frequency response of the hot-wire system was found to be approximately 100 kHz, and data were analyzed with a relevant calibration. The velocity-voltage relationship was assumed to follow a fourth-order polynomial. The calibration procedure required variation of velocities and inclination angles. Twenty-eight velocities covering the entire range anticipated were chosen, and at each velocity the probe was yawed 17 times to cover the angles from -40 to $+40$ deg. Thus, because of the hot-wire calibration equation and data acquisition, the uncertainty of the mean velocity was less than 2% and of the fluctuating velocity 5%. Control of the injected air temperature was carried out by a K thermocouple with a 0.5°C accuracy, which allows us to evaluate the sound velocity a with a 0.08% accuracy. Finally, some pictures of the flow were taken through a visualization technique. Heated oil, vaporized into smoke and injected through a slot between the second and the third block, reflected a 10-mJ-power copper vapor pulsed laser light and pictures were captured by a 16-mm Nac ultra-high-speed camera, recording 8000 images per second. This visualization technique provided qualitative and quantitative information on shear-layer development.[13]

III. Coupling Phenomenon Detection

Periodic shedding of vortices induces a source of substantial acoustic energy in highly sheared flows, potentially able to generate unstable conditions in the flow itself. Flandro and Jacobs[14] were the first to suggest that pressure oscillations could be generated by vortices resulting in acoustic instabilities in some propellant rocket motors. Indeed, experimental studies carried out with cold gas apparatuses demonstrated that vortex shedding from restrictors is coupled with the acoustics of the chamber so as to generate substantial acoustic pressure levels. The maximum amount of acoustic energy is produced when the shedding frequency matches that of the acoustic mode of the chamber. Then, to detect the presence of a coupling phenomenon in the flow, several tactics may be employed. The first and the easiest is to characterize the pressure fluctuations in the chamber. In fact, with firing propellant rocket motor test, it is the only way; because of high pressure and high temperature, no other measurements are possible. A correlation between the frequency response in the fluctuating pressure spectrum and the acoustic mode of the chamber has to be made. Recently, Scippa et al.[3] reported analyses of the full-scale firing results of the pressure oscillations in the Ariane 5's solid propellant motor. The main part of fluctuation energy is concentrated near the first longitudinal acoustic mode of the chamber. The observation can also be made with cold gas simulation. For instance, Brown et al.[15] showed a significant increase in acoustic pressure for a given Mach-number range in the chamber, and this increase is accompanied by clearly audible tones not observed at the other Mach numbers. Couton et al.[11] also reported a phenomenon of selective excitation in the neighborhood of the first longitudinal acoustic mode. It manifests itself by a "frequency jump" accompanied by energy transfer from one mode to another. Nevertheless, all of these experiments pointed out the presence of a form of interaction between hydrodynamics and acoustics, which could represent just a resonant phenomenon and not a real coupling phenomenon. For example, Vetel et al.[16] recently indicated that an increase of the characteristics velocity u_v in a cold gas chamber is followed by an increase in the vortex-shedding frequency from restrictors. In some experimental configurations the chamber acts as a resonator. In such cases energy accumulation is negligible, and an edge tone phenomenon takes place when acoustic resonance occurs at a fixed frequency. In other words, if there is no receptivity of the hydrodynamic flow, no energy transfer from acoustics to hydrodynamics develops and interferes with the unstable behavior of the internal flow. As stated by Ho and Nosseir,[17] a feedback phenomenon can create interaction from acoustics to hydrodynamics. This mechanism was clearly identified both in open and in confined areas. Trailing edges, rings, cylinders, baffle configurations[18–20] were widely studied in the beginning of the 1980s. Findings suggested that interaction between the fluid and the obstacle is the primary cause of acoustic wave emission and leads to strong amplification of the pressure field. In certain cases the acoustic waves, moving upstream toward the origin of the shear layer, can maintain the generation of vortex structures and strengthen coherence and energy of structures. The instabilities are then sensitive to the waves, which they have indirectly generated. Such instabilities are mainly characterized by a Strouhal number, remaining at a constant level in a given velocity range. This clearly indicates that unstable frequency and hydrodynamics are coupled, in which case a feedback loop forces acoustic control on the vortex-shedding frequency. In such cases correlation measurements between the fluctuating velocity field and the fluctuating pressure field can be decisive in attempts to demonstrate the presence of the feedback loop phenomenon.

Figure 2 presents characteristic changes of the correlation coefficient $R_{u'P'}(\tau)$ with time τ between the front-head pressure fluctuations and the velocity fluctuations recorded at ($X = 0.637$, $Y = 0.90$), i.e., in the wake of the obstacle. Measurements were made for various Mach numbers at a specific $Re = 1.45 \times 10^5$. First, $R_{u'P'}(\tau)$ is mainly characterized by a trigonometric shape underlining that pressure fluctuations are organized around discrete frequencies. A signal envelope $A(\tau)$ of $R_{u'P'}(\tau)$ was also plotted, allowing for a more accurate estimation of the correlation time delay τ. For instance, at $M = 0.100$ no organized correlation in time is observed even if $R_{u'P'}(\tau)$ reaches approximately 10% at a negative time delay. Nevertheless, $R_{u'P'}(\tau)$ are highly sensitive to the Mach levels. The higher the Mach number, the greater the $R_{u'P'}(\tau)$ correlation coefficients, Second, it is clearly evident that pressure fluctuations and velocity fluctuations are correlated as well at a negative time delay τ^- as at a positive time delay τ^+. For $M = 0.143$ the highest correlation is 24% at τ^-, and a weak correlation at τ^+ is also present. These levels increase with regard to M. Correlation of 27% and 10% are, respectively, reached at τ^- and τ^+ for $M = 0.167$. As described in recent work[16] and considering the location of the sensors, correlation at τ^- underlines the fact that pressure fluctuations occur prior to velocity fluctuations because it can be assumed that pressure waves directly influence vortex shedding in the wake of the obstacle. Indeed, if a pressure wave creates a forced oscillation in the shear layer resulting in the formation of a coherent eddy, this pressure wave will continue its propagation at a velocity close to the sound traveling velocity a, modified by the flowfield

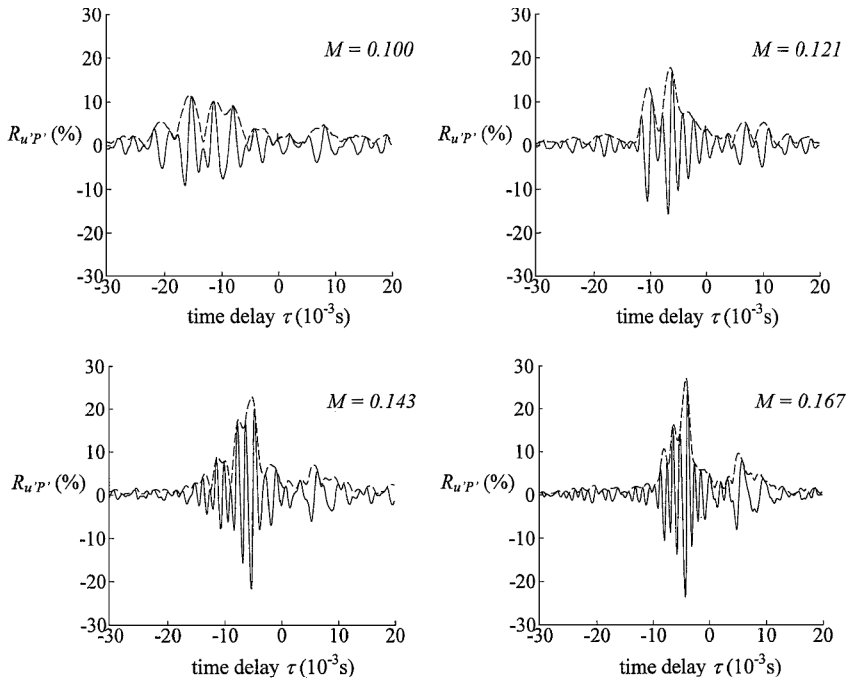

Fig. 2 Change of $R_{u'P'}(\tau)$ vs Mach number at $Re = 1.45 \times 10^5$: ——, correlation coefficient, and – – –, signal envelope.

velocity itself. Even if correlation at τ^+ is not as considerable, a correlation is detected. Indeed, this can be explained because the information is delayed in time for the pressure at the front head. In fact, a coherent structure is convected from the restrictor location to the submerged nozzle location, where the impingement of the structure creates a significant noise. A pressure wave is then created traveling upstream of the flow toward the front-head location. The correlation obtained at τ^+ underlines the interaction of the nozzle and impingement of structures, acting as a source of noise and as a feedback loop control. τ^+ in fact physically represents the feedback loop of the vortex-shedding phenomenon. As stated by Vetel et al.,[16] an analytical model can be used for an evaluation of both negative and positive time delays. τ^- and τ^+ can be expressed as (see Fig. 1)

$$\tau^- = d_0/u_c - d_1/(a - u_v) \tag{3}$$

$$\tau^+ = d_2/u_c + d_3/(a - u_v) \tag{4}$$

Then, even if characteristic velocity increases along the channel, the convection velocity of structures is assumed to be equal to 60% of the mean velocity level u_v. In fact, Ho and Nosseir[17] found the convection speed of the large coherent structures to be 0.6 of the jet exit speed. Lau et al.[21] and Neuwerth[22] confirmed this value, respectively, in a low-speed jet and in a high-speed jet.

To estimate Reynolds-number influence over correlation, measurements were made at various Reynolds numbers at the same fixed hot-wire location, and Fig. 3 presents all of the time correlation coefficients obtained. With the assumptions just listed equations of τ^- and τ^+ time delays were computed at the same location for velocity measurements as those of the experiments. Results are also shown by the dotted line on Fig. 3. To do this, we first assume the presence of the feedback loop at every velocity range studied so that expressions of τ^- and τ^+ have a physical meaning.

Figure 3 underlines the fact that beyond the threshold level of $M_0 = 0.09$ a characteristic agreement was reached between experiments and analytical values of time delays, both negative rather than positive time delays for all Reynolds numbers studied. It must be recalled that the higher the Reynolds number, the larger the range in which a significant correlation at τ^- and τ^+ is observed. At $M < M_0$ the $R_{u'P'}(\tau)$ levels reached were not as significantly high, which indicates noncoupling of the velocity and the pressure fields. In other words, if vortices are present in the wake of the obstacle, their frequency was not forced by the acoustic. At the same time for $M \geq M_0$ the coupling phenomenon was present in the flow. In such conditions it is important to study pressure amplification with regard to Reynolds and Mach numbers as well as selective energy transfer between modes.

IV. Pressure Field

A. Amplification: Effect of Reynolds Number

The behavior of the normalized rms pressure is analyzed in Fig. 4 with regard to M and parameterized with Re, i.e., the injected mass flow rate. It must be underlined that these levels are an order of magnitude smaller that levels measured in the full-scale motor.[1] According to previous simulations,[7,10,15,23] cold gas simulations failed to reproduce such levels. In fact, it is important to point out that such simulations were conducted in order to explain the fundamental phenomena of unstable behavior. Moreover, as stated Sec. II. A, simulations were based on some simplifying assumptions like for instance the none Reynolds number similitude, which would explain the difference in the pressure levels between cold gas experiments and solid propellant motor firing. The highest level reached is 0.09% for $M = 0.23$ at the highest Reynolds number studied. Levels of $\sqrt{P'^2}/P$ are strongly sensitive to Re as well as M, and their amplification can be described by two or three amplification stages. For the lowest Reynolds-number levels studied ($Re \leq 1.29 \times 10^5$), two different amplification stages are mainly characterized by a linear increase. For instance, at $Re = 0.86 \times 10^5$ the increase of $\sqrt{P'^2}/P$ with regard to M is linear from $0.05 \leq M \leq 0.09$, and beyond 0.09 a second stage of amplification is present with a higher slope. For higher Reynolds-number levels we observe three amplification stages in which three different linear slopes characterize the increase of $\sqrt{P'^2}/P$. This is clearly identified at $Re = 1.29 \times 10^5$. At this level and for $0.07 \leq M \leq 0.09$, the increase of $\sqrt{P'^2}/P$ corresponds to that obtained at lower Reynolds numbers. Then, another stage of amplification is reached for $0.10 \leq M \leq 0.14$, and finally a third is observed for $M > 0.14$. For the highest Reynolds numbers studied once again just two stages of amplification are observed. This is because of the lowest Mach-number level available for this Reynolds number (Table 1) because the Mach-number range is directly linked to the injected mass flow rate, i.e., to the Reynolds-number level. To see the overall picture, in occurrence with the coupling phenomenon, amplifications in the pressure fluctuating field are observed with the increase of Mach number whatever the level of the Reynolds number. Nevertheless, the influence of Reynolds number is significant: the higher the Reynolds-number level, the more the noise amplifies in the chamber. To better understand the

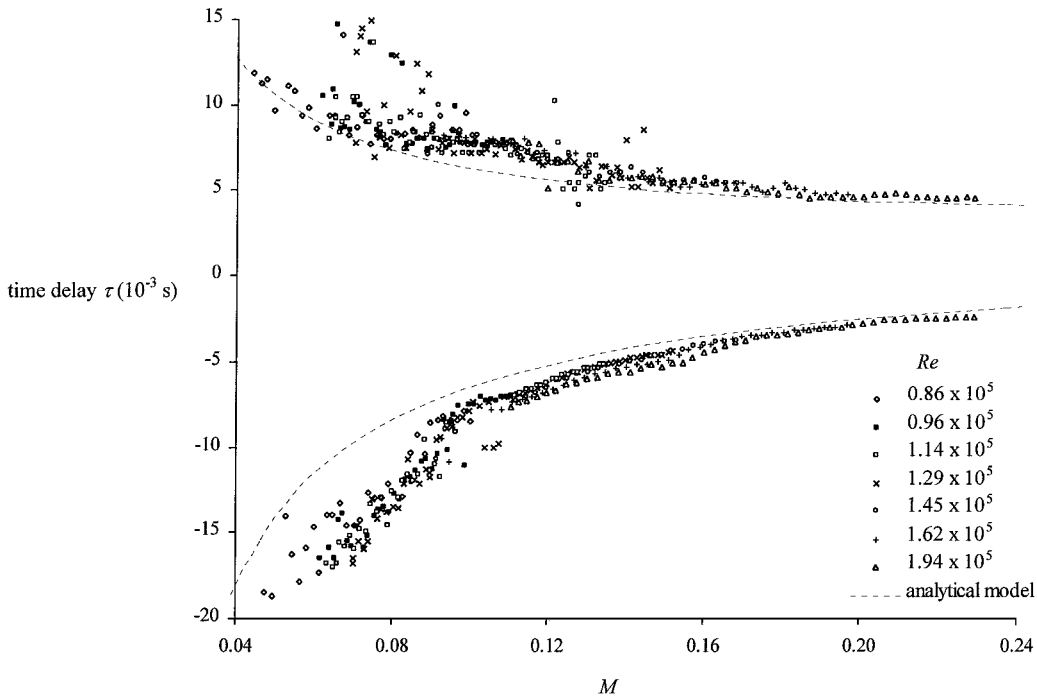

Fig. 3 Comparison between experimental and analytical results of time delay τ vs Mach number with regard to Reynolds-number level.

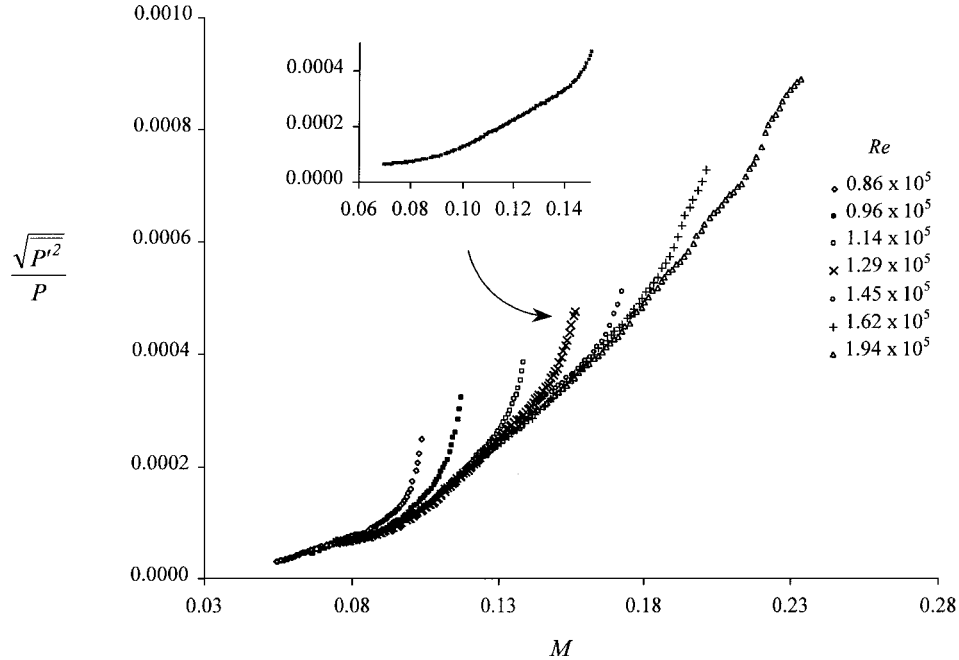

Fig. 4 RMS of pressure fluctuations at head end vs Mach number with regard to Reynolds-number level.

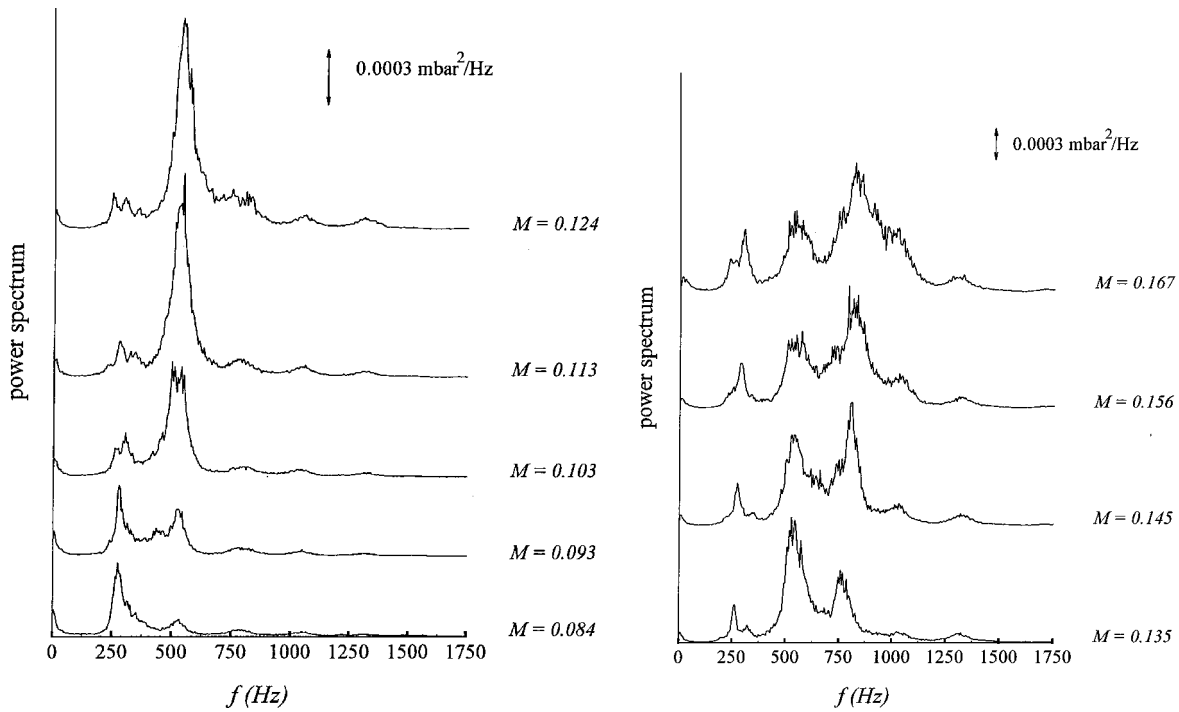

Fig. 5 Change of the pressure spectral response vs Mach number at $Re = 1.45 \times 10^5$.

amplification stages and to determine whether a coupling phenomenon generates important energy levels, spectral analysis of the pressure fluctuations was performed.

Some characteristic spectral responses of the pressure fluctuating field are displayed in Fig. 5 for $Re = 1.45 \times 10^5$ obtained at different Mach-number levels. At $M = 0.084$ the power spectral density is characterized mainly by a dominant peak close to 270 Hz. The comparison of the resonance frequency with the closed-closed acoustic theroretical modes of the chamber (f_{1L}), based on the channel length L, confirms an agreement with the inner acoustic of the chamber. With higher Mach-number levels the second longitudinal acoustic mode (f_{2L}) can also be excited. For $0.103 \leq M \leq 0.124$ it becomes by far the most energetic mode. Beyond $M = 0.135$ the third longitudinal acoustic mode f_{3L} is present in the spectral response, and at the highest Mach number reached for $Re = 1.45 \times 10^5$, f_{3L} concentrates the main part of fluctuating energy. A weak concentration of energy is detectable at the fourth longitudinal acoustic mode, but f_{1L} and f_{2L} are still present. So in these conditions the first four acoustic modes can be excited at the front head of the chamber. To quantify the phenomenon of energy transfer in the pressure fluctuations, several series of measurements were carried out in a wide range of Reynolds-number levels and in the complete Mach-number range. Results obtained, for four Reynolds-number levels, are given in a pseudo-three-dimensional power spectral density as function Mach number in Fig. 6.

The increase of Reynolds number generates progressive excitation of acoustic modes from the fundamental toward highest harmonics. For instance at $Re = 0.86 \times 10^5$, f_{1L} is the most excited frequency for $0.05 \leq M \leq 0.09$. For $M > 0.09$, f_{2L} abruptly appears in the spectrum even if f_{1L} is always the highest excited

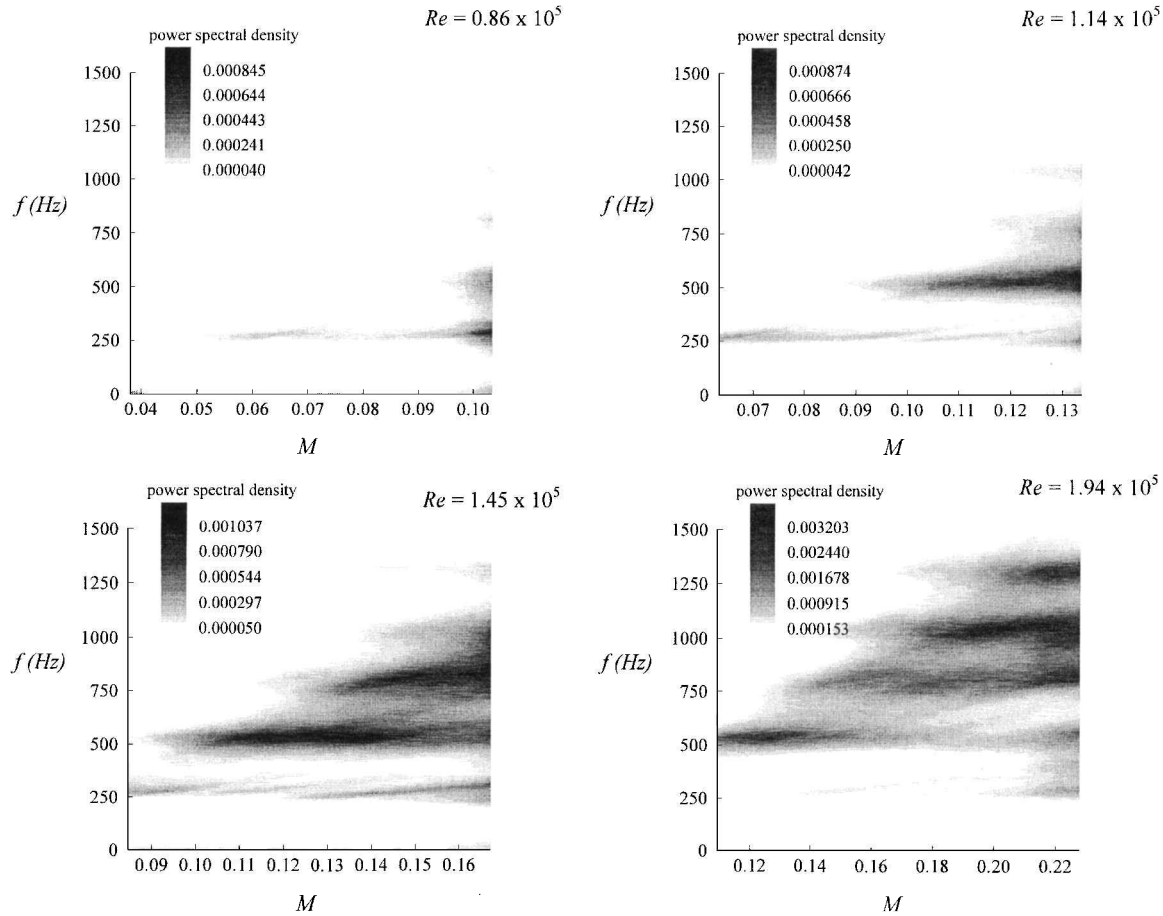

Fig. 6 Change of the magnitude and frequency of the most energetic frequency with regard to Mach number at different Reynolds-number levels.

mode. At $Re = 1.14 \times 10^5$ there exists the same behavior in the same Mach-number range, but as M increases, f_{2L} is predominant until $M = 0.11$, and its energy level amplifies strongly. For $Re = 1.45 \times 10^5$ beyond $M = 0.11$, its energy level decreases concurrently with the increase of M. Then, f_{1L} and f_{3L} appear in the spectrum, but f_{3L} repidly increases and becomes the highest excited mode. In fact, the higher the Reynolds number, the higher the harmonic mode that can be excited. Each mode is successively excited from the fundamental mode to the harmonics, becoming predominant in the spectral response as for example at $Re = 1.45 \times 10^5$ (f_{2L}, f_{3L}, and f_{4L}) at $Re = 1.94 \times 10^5$ (f_{2L}, f_{3L}, f_{4L}, and f_{5L}). This also underlined that no transversal and lateral modes were excited. The favored excitation of one or several modes is mainly driven by the Reynolds-number level as well as Mach-number level. Couton et al.[10] underlined that a phenomenon of selective excitation of the first acoustic modes occurs; it manifests by a frequency jump and is accompanied by energy transfer from one mode to the other. This mechanism is observed from the fundamental frequency to a higher one corresponding to a phase of growing modes. Although higher harmonic modes are dominant in the spectral response, it is also clear that low frequencies (f_{1L} and f_{2L}) are always present in the energy distribution at the front head of the chamber. As already seen, internal acoustics is therefore sensitive to flow parameters. Amplification of the pressure fluctuations could be caused by the coupling between the acoustic field and the vortex field, as stated in the preceding correlation study. At which frequency are structures shed and does the dominant resonant frequency really indicate the coupling frequency? Indeed, it is necessary to clarify the role of acoustics on the coupling phenomenon. To do so, a close study of the excited frequency is required.

B. Self-Sustained Oscillation Mechanism

Although we concentrate on the amplification levels of the pressure fluctuations as well as the excited frequencies in the spectral response, it may be of decisive importance to closely follow at which frequency a mode is excited. To do so, all spectra containing an energy concentration in the neighborhood of the fundamental mode were used to display the frequency with regard to the Mach number and the Reynolds number (Fig. 7a). The complete data obtained clearly reveal some linear evolution with regard to the Mach-number increase whatever the Reynolds-number level. In fact, under $M = M_0$ no particular evolution of the emerged frequency is detectable. On the contrary, the excited frequency remains close to f_{1L}. Then, for $0.09 \leq M \leq 0.11$ the frequency increases concurrently with the increase of Mach number. The change is detectable at any Reynolds-number level. In this first stage the excited frequency varies from 260 to 320 Hz. At $M = 0.11$ an abrupt jump of the excited frequency occurs followed by another linear increase of f_{1L} with M. This second stage ($0.10 \leq M \leq 0.13$) reveals approximately the same evolution of the frequency as in the first. After another jump at $M = 0.12$, a third stage is observed but with a higher frequency range (235–350 Hz) and is more lengthy in the Mach scale ($0.116 \leq M \leq 0.195$). Then, a last jump between the third and the fourth stage is not as clear as the others. Indeed, the last stage ($0.175 \leq M \leq 0.23$) contains fewer data simply because it corresponds to the highest Reynolds number studied. Furthermore, a type of hesitation can be underlined by the fact that at $Re = 1.98 \times 10^5$ the highest excited frequency successively reaches the third and the fourth stages. Indeed, each range in which a linear increase of f_{1L} is detected overlaps. This could represent a kind of hysteresis effect on the linear coupling. Nevertheless, no such evolution can be traced back following the variation of the excited frequency close to the second acoustic mode f_{2L} (Fig. 7b). In fact, the change of f_{1L} clearly indicates an edge-tone phenomenon in which Strouhal number remains constant coupled with a resonants phenomenon.

The Strouhal number was introduced in order to characterize the unsteady phenomena in flows. Soreefan[24] and Flatau,[25] for instance, assimilate the Strouhal number with reduced frequency of vortex-shedding phenomenon. It can be effectively connected to

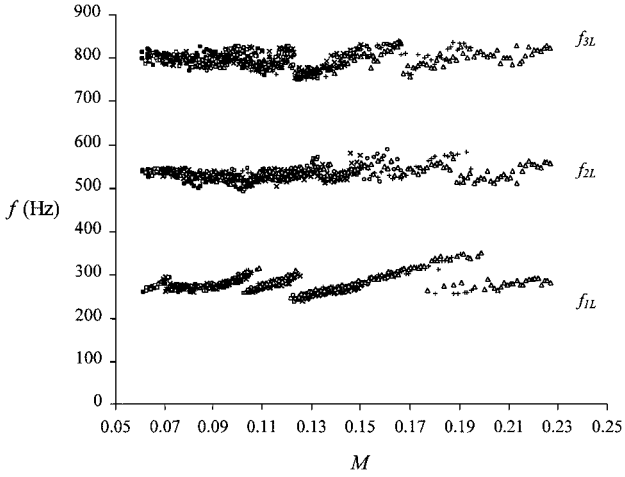

Fig. 7a Frequency evolution in the pressure spectral response at head end vs Mach number and for the complete Reynolds-number range.

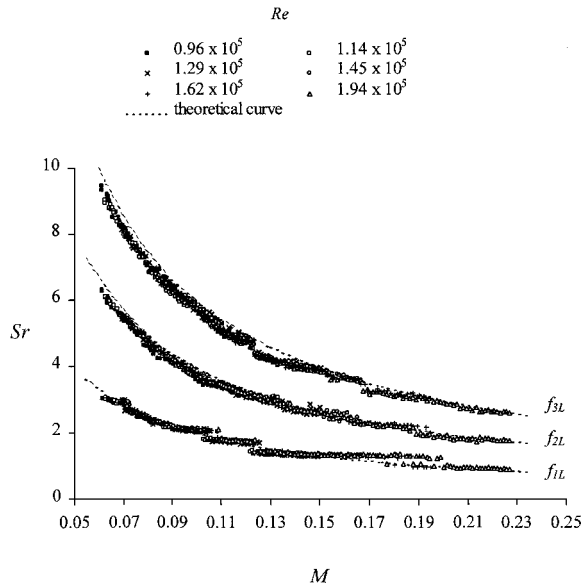

Fig. 7b Strouhal-number change with Mach number in the complete Reynolds-number range.

hydrodynamic instabilities and the internal pressure fluctuations they generate. In fact, it can be defined in different ways, but concerning an unstable shear-layer development the Strouhal number is generally based on shear-layer thickness or on the distance between the separation location of structures and their impingement. So, in this case, considering the frequency of the first acoustic mode f_{1L}, the relationship Mach number–Strouhal number is written as

$$Sr = f_{1L}l/aM \tag{5}$$

Figure 7b displays the change of Strouhal number with regard to Mach number at every Reynolds-number level studied. The general shape roughly shows that the change of Strouhal number as a function of Mach number is actually a hyperbola. Nevertheless, data underline the presence of four different stages in which Strouhal number remains at a practically constant level. First, hydrodynamics conditions must have a characteristic Mach number higher than the threshold level, $M_0 = 0.100$ in order to display such constant Strouhal-number evolution. Second, it demonstrates that a coupling does not necessarily organize itself at the highest excited acoustic mode. It can be explained by an inability to adjust to acoustic-hydrodynamic fields. This notion will be developed hereafter. Finally, the coupling phenomenon introduces an acoustic-hydrodynamic mixing effect in the flow with a resonant state at a quasi-fixed frequency followed by several constant Strouhal stages in the neighborhood of the acoustic frequency.

As noticed by Jones et al.,[26] acoustic-hydrodynamic mixing effects are often present. In their experimental results oscillations close to the first longitudinal acoustic mode appeared at a fixed frequency while those at higher modes revealed successive constant Strouhal-number stages with regard to flow velocity. In our case, constant Strouhal-number stages are well-identified close to f_{1L}. The changes of f_{2L} with M do not underline any particular organized evolution. On the contrary, Fig. 7a clearly indicates that in the vicinity of f_{2L} resonance occurred at a fixed frequency or at least in a small frequency range around f_{2L}. The figures depict approximately the same behavior at a higher acoustic mode (f_{3L}) despite a weak linear evolution of f_{3L} for $0.12 \leq M \leq 0.16$. Amplification in the fluctuating pressure field is observed with regard to Reynolds and Mach number. This amplification is caused by a coupling phenomenon between acoustics and hydrodynamics. The energy involved suffices to excite the first four longitudinal acoustic modes of the chamber. Nevertheless, the coupling phenomenon seems to match up with f_{1L} though this frequency is not the higher excited frequency in the spectral response. In view of enhanced understanding, a close study of the shear layer would be of decisive importance.

V. Shear-Layer Development

Thanks to the development of visualization techniques, the destabilization of the shear layer was analyzed recording a 8000-Hz cadence film. Figure 8 presents four successive pictures in which the creation and the roll up of a structure can be identified. In the $X = 0.2$ length available frame two different roll-up motions can be observed. The first one, closer to the obstacle, convected itself in the wake of the obstacle, whereas with the second, a clear up-and-down motion is detectable. In fact, the second roll up in the picture is not as seeded as the first one. This was caused by the nonconstant light-sheet laser intensity along the X available frame. The up-and-down motion underlines the pulsation of the shear layer. A quantitative approach,[13] based on the numerization of the film and its treatment, makes it possible to characterize the frequency of the vortex-shedding phenomenon. Although a f_{1L} frequency was clearly detectable in the spectrum, the spectral response was mainly noised neither by turbulence nor by the seeding system itself. In fact, the seeding flow, injected upstream of the obstacle, generated an unsteady flow as a result of the presence of pressure oscillations in the chamber. This disturbed the shear-layer seeding and precluded a quantitative analysis through visualization. In these conditions a complete investigation was performed by hot-wire measurements.

Upstream of the obstacle location, the flow organizes like a well-known wall injection flow in which longitudinal and transverse velocity components fit the analytical trigonometric law of Taylor.[10] Furthermore, in such flow without any geometric discontinuities, wall injection stabilizes the flow and decays the turbulence phenomenon appearance. So, despite a relatively high Reynolds number, the flow is laminar upstream from the obstacle location. On the other hand, experimental velocity measurements show dynamic disturbances of the flow downstream from the obstacle location. Longitudinal velocity profiles u, turbulence intensity profiles It, and shear-stress $\overline{u'v'}$ profiles are plotted in Fig. 9 for some longitudinal X values. Results shown in Fig. 9 were obtained for $Re = 0.86 \times 10^5$ and $M = 0.096$. Only a few profile sections are plotted, but the results omitted do not change the layout. The mean flow is mainly characterized by two areas. The first one, located close to the obstacle location, features significant shear development. The shear layer develops by the mixing of the main flow, which passes over the top of the obstacle, and of the injected flow, which passes through the porous wall downstream from the obstacle location. The second area pattern does not present such significant longitudinal transverse gradients but is highly dependent on the first one. In fact, profiles are marked by an inflexion point as for instance at $X = 0.32$ and 0.40. Closer to the rear end, inflexion point does not characterize the profiles, and shapes are comparable to those upstream from the obstacle location. Nevertheless, as underlined by the change of It in the wake of the obstacle, the flow becomes turbulent. For instance, at $X = 0.08$ turbulence intensity It reaches a maximum higher than 15% but quite rapidly the turbulence spreads toward the injected

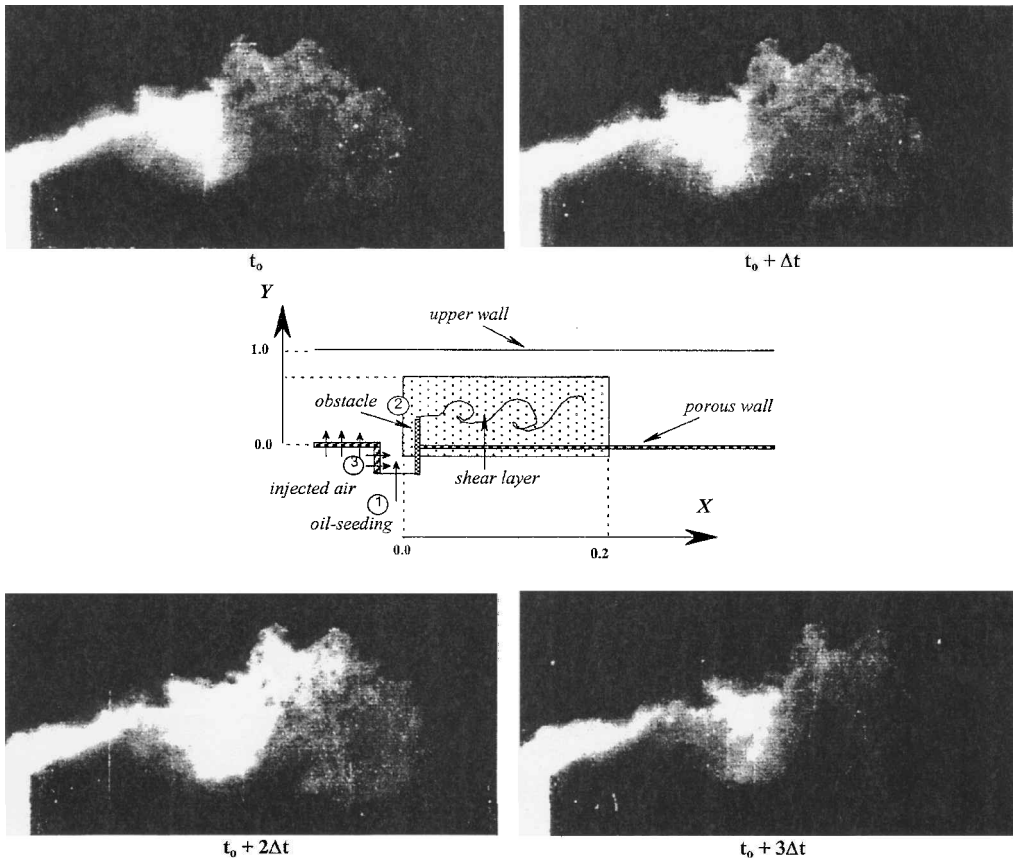

Fig. 8 Visualization of the shear-layer destabilization at 8000-Hz frequency.

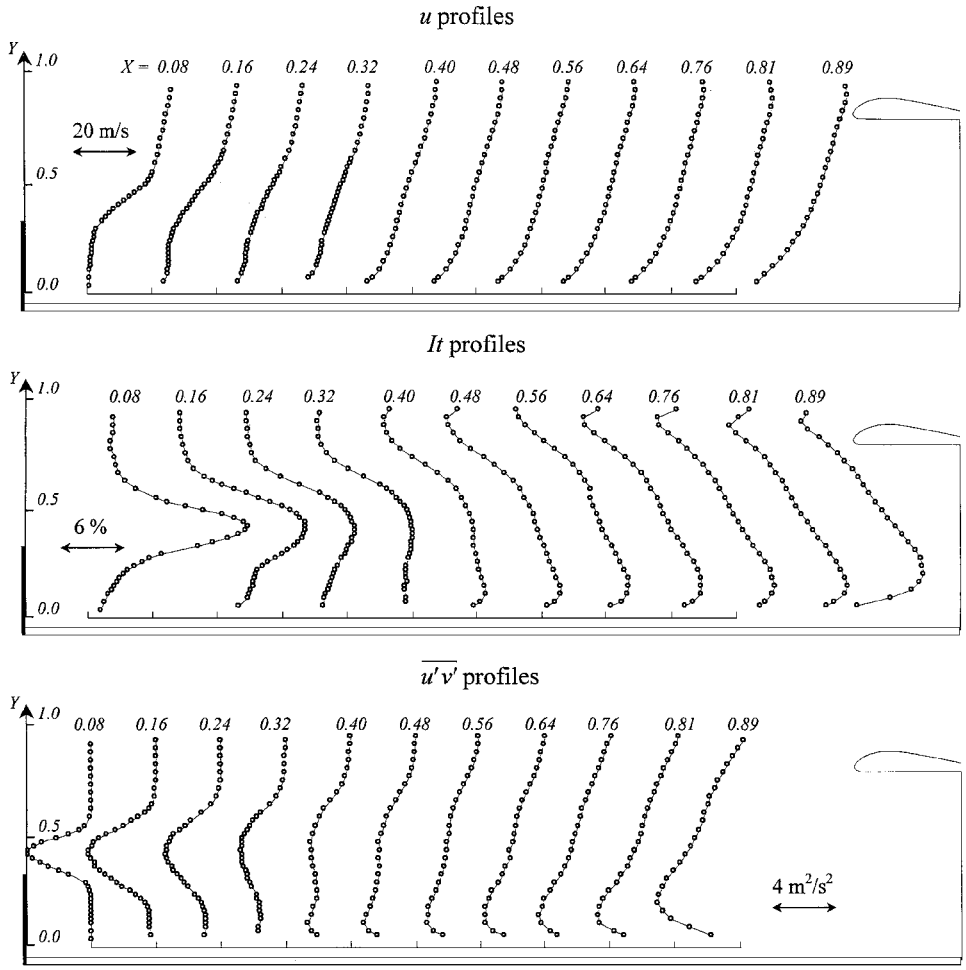

Fig. 9 The *u* velocity component and turbulence (*It* and $\overline{u'v'}$) profiles downstream from the obstacle location.

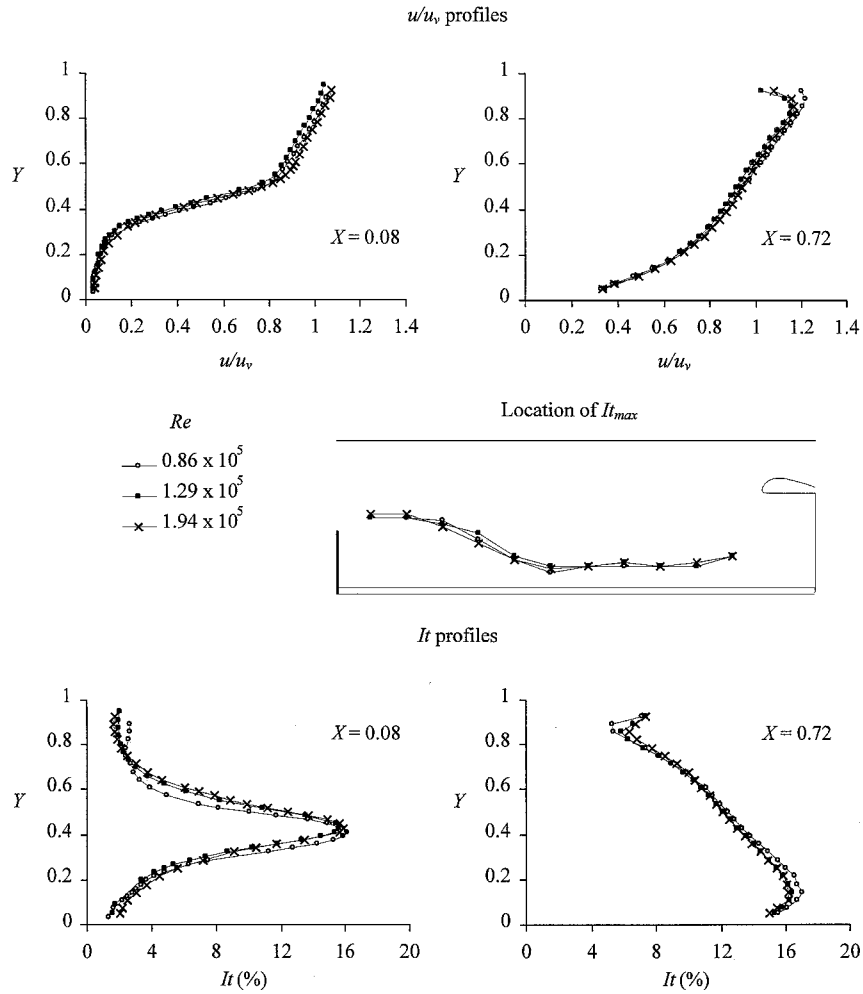

Fig. 10 Comparison of nondimensional u/u_v, velocity component and *It* with regard to three Reynolds-number levels in the separation area ($X = 0.08$) and in the rear-end area ($X = 0.72$).

walls to such a point that the maximum of *It* is reached close to the latter for $X \geq 0.40$. Beyond this location, the transverse maximum location decays from $Y = 0$ with regard to X. For instance, $It_{\max}$ is reached for $X = 0.48$ and 0.89 at $Y = 0.1$ and 0.25, respectively. Shear-stress measurements start off strongly in the obstacle's wake with levels at about -4 m^2/s^2. Profile shape in the vicinity of the obstacle location is mainly characterized by a minimum peak of $\overline{u'v'}$ indicating that, at the origin of the shear layer, the shear creates important turbulence. The $\overline{u'v'}$ profile shapes change progressively with the same characteristics as *It* shapes. It is clearly evident that turbulence develops itself close to the injected wall at $X = 0.40$ and that the intensity of the $\overline{u'v'}$ minimum increases with regard to X. Indeed, the flow becomes highly turbulent downstream from the obstacle location, and the role of the injecting walls seems to be noteworthy.

To compare the Reynolds-number effect, measurements were carried out for two other Reynolds-number levels at a fixed front-head pressure, i.e., at different Mach-number levels (Table 1). Figure 10 allows us to compare normalized longitudinal velocity u/u_v, and turbulence intensity *It* profiles in two different locations downstream from the obstacle location with regard to the Reynolds number. In the vicinity of the obstacle ($X = 0.08$), the shape of velocity and turbulence profiles are similar; the higher the Reynolds number, the higher the normalized velocity above the top of the obstacle ($Y \geq 0.32$). In the rear part of the channel ($X = 0.72$), even if profiles still present similar shapes, the Reynolds number tends to favor a higher turbulence intensity close to the wall injection. $It_{\max}$ is obtained at the same transverse location ($Y = 0.12$), but levels do not depend strongly on the Reynolds number. These measurements underline the fact that the shear-layer development is not highly sensitive to the Reynolds number, i.e., to velocity itself. This is caused by a shear layer creation, which comes about through a mixing of the main flow passing above the obstacle and of the wall injection flow. As the Reynolds number increases, the velocity of each part of the mixing flows increases as well, and no particular change of the flowfield is induced. We focused this study on the effect of Reynolds-number influence, which had a very sensitive effect. Then, it is necessary to underline that we performed a simulation of a full-scale solid rocket motor with a characteristics Reynolds-number range an order of magnitude smaller than those observed in solid rocket motor. Nevertheless, turbulence transition in injecting wall flows depends not only on the Reynolds number but also on the Reynolds numbers of the main flow with regard to the injecting Reynolds number. Moreover, which is the key point, turbulence in our flow appears not because a laminar toward turbulence transition but because of the obstacle emergence creating an intense shear layer.

To conclude our remarks on the unstable behavior of the flow, fluctuating velocity field was closely studied. Figures 11 and 12 respectively present the spectral distribution in the fluctuating velocity at four Reynolds-number levels obtained in two different areas: 1) in the vicinity of the obstacle position and 2) in the rear end of the chamber. It enables us to follow the dominant frequency in the vortex-shedding area and its change in the whole chamber.

At the lowest Reynolds number studied ($Re = 0.86 \times 10^5$), it is clearly evident that in the vicinity of the obstacle location, i.e., in the separation region (Fig. 11a), the most excited energetic frequency increases linearly with Mach number going up from 0.040 to 0.075. The vortex-shedding phenomenon is driven by one main frequency. According to stability analysis in the wake of an obstacle,[24,25] it is well known that hydrodynamic conditions lead to structure generation and that the higher the velocity the higher the vortex-shedding frequency. In the same Mach-number range fluctuating

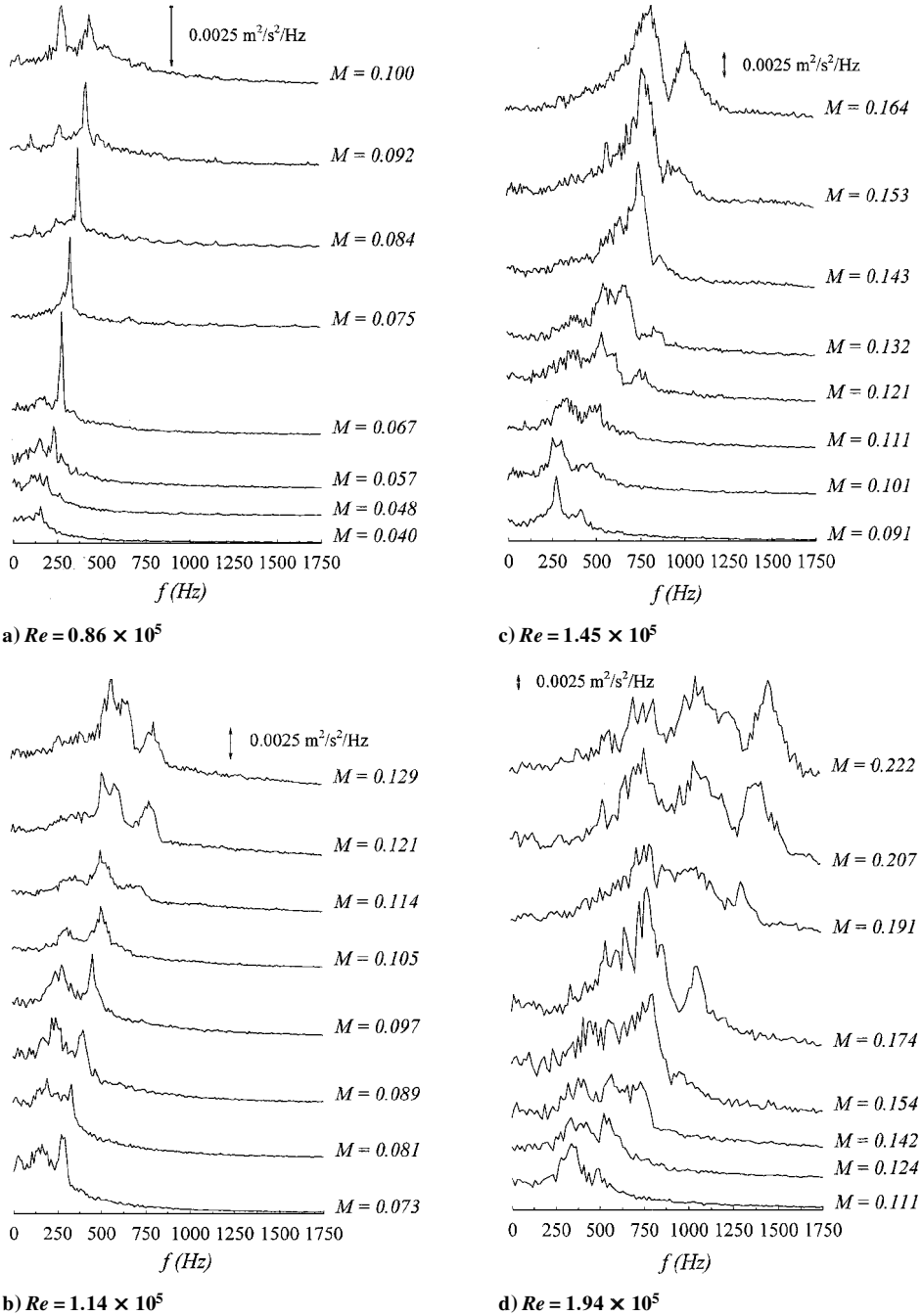

Fig. 11 Change of spectral analysis of fluctuation velocity component in the separation area ($X = 0.16$, $Y = 0.58$) with Mach number for four Reynolds-number levels.

velocity spectra do not present any particular energetic organization around a given frequency at the rear end of the chamber (Fig. 12a). This demonstrates that structures created in the separation area lose their coherence on their way from the obstacle position to the submerged nozzle location. Structures created at a specific hydrodynamic frequency are dissipated by either turbulence or interference with wall mass transfers or vortices; they are not sufficiently powerful to keep up their own coherence. Nevertheless, at $M = 0.084$ a dominant peak is observed at both $X = 0.16$ and 0.65. This indicates that in these conditions structures are still present in the shear layer and that they impinge on the nozzle then create significant noise. Moving upstream toward the origin of the shear layer, pressure waves set the vortex-shedding frequency at the obstacle location and strengthen these structures by disrupting velocity and hydrodynamic frequency. As shown in Fig. 11a, vortex-shedding frequency suddenly jumps from 480 to 270 Hz, i.e., close to f_{1L} first acoustic longitudinal mode. This underlines how coupling between acoustics and hydrodynamics proceeds. Figures 11b and 12b show spectral responses of the fluctuating velocity field in the two areas for $Re = 1.14 \times 10^5$. Energy is concentrated at a specific frequency close to f_{1L} at $M = 0.073$ in the separation area (Fig. 11b), and this frequency increases with regard to Mach-number levels in the chamber. For instance, at $M = 0.089$ the dominant frequency in the velocity spectra is close to 340 Hz and increases linearly up until $M = 0.114$. As the dominated frequency in the pressure field is always close to f_{1L} in that Mach-number range, Fig. 12b indicates that vortices are organized around f_{1L} in the rear end of the chamber. Even if structures are shed at a higher frequency, the resulting frequency is close to f_{1L}. Furthermore, at times spectra have one peak in the neighborhood of f_{1L} ($M = 0.097$) and other times two peaks ($M = 0.114$). Following the shape in the spectral response, these two peaks seem to be in rivalry with each other and compete to be the higher one; the same behavior is observed closely following the change of the frequency in the pressure field. To understand this behavior, it is important to remember that characteristic acoustic pressure and acoustic velocity are modified throughout the chamber.

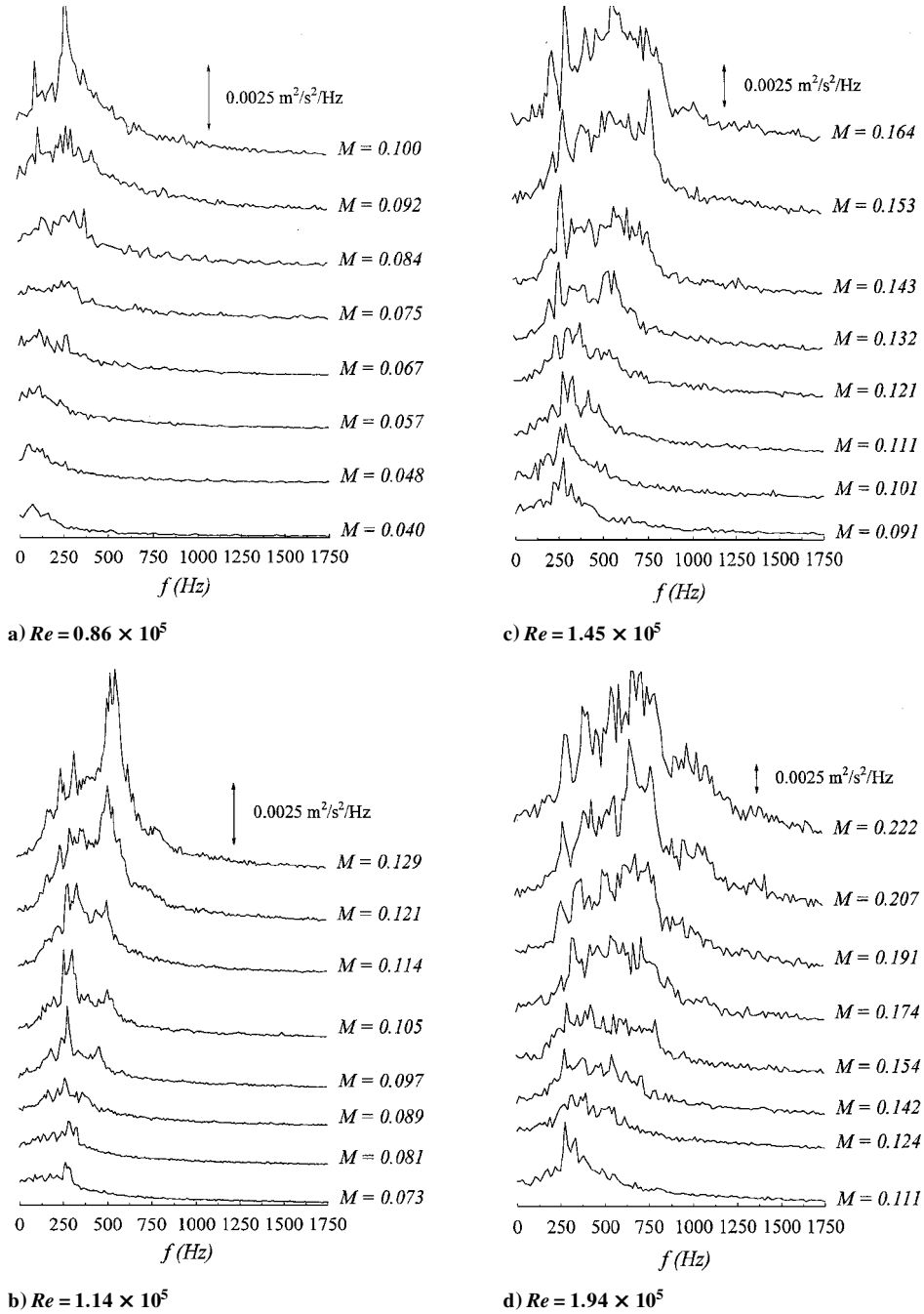

Fig. 12 Change of spectral analysis of fluctuation velocity component in the separation area ($X = 0.65$, $Y = 0.89$) with Mach number for four Reynolds-number levels.

In the wake of the obstacle, a pairing of two structures occurs and decreases the characteristic frequency, actually divided by 2. This would indicate emerging frequency in the 130–270-Hz range. As Fig. 12b only depicts frequencies close to f_{1L}, this shows that acoustic conditions force the pairing frequencies to match up with f_{1L}. For $M \geq 0.114$ the dominant frequency remains close to f_{2L} in the obstacle area (Fig. 11b) even if M increases while f_{2L} becomes by far the most dominant frequency. In these dynamic conditions structures are shed close to f_{2L} and keep their own coherence until they reach the rear end of the channel. The coupling phenomenon organizes itself at f_{2L}, whereas f_{1L} frequency corresponds to the presence of a pairing phenomenon. At a higher Reynolds number ($Re = 1.45 \times 10^5$) spectra are mainly characterized by f_{1L} and f_{3L} frequencies. At the obstacle location structures are organized close to f_{1L} for $M \leq 0.101$, and as M increases the dominant peak quickly shifts toward f_{3L}, which becomes by far the most powerful frequency. In this configuration frequencies rapidly shift from f_{1L} to f_{3L} without any particular organization around f_{2L} when M increases. This is as a result of the obstacle location in relation with the whole length of the chamber. Acoustic conditions do not favor f_{2L} in the wake of the obstacle: f_{2L} decreases in the acoustic pressure amplification and is at a low level for acoustic velocity because the velocity node is close to the obstacle location. Spectra in the rear end of the chamber (Fig. 12c) are highly disturbed and yet still driven by frequencies close to f_{1L} in the complete Mach-number range available. This once again underlines the complex flow organization in which acoustics force instabilities close to f_{1L} even if pressure excites higher longitudinal modes. For the highest Reynolds number presented (Figs. 11d and 12d), the noised spectra render it quite difficult to analyze a clear defined trend. Nevertheless, structures are shed at different frequencies: for $M = 0.111$ the dominant peak is centered at f_{1L}, and at $M = 0.174$ it is close to f_{3L}. For $M \geq 0.191$ the frequency domain is very large, and energy is concentrated at f_{2L}, f_{4L}, and f_{5L} in the vicinity of the obstacle location. As just mentioned, the spectra in the rear end of the channel are always characterized by lower frequencies close to f_{1L} and f_{3L}. This demonstrates the presence of a phenomenon forcing the characteristic vortex-shedding frequencies to decrease.

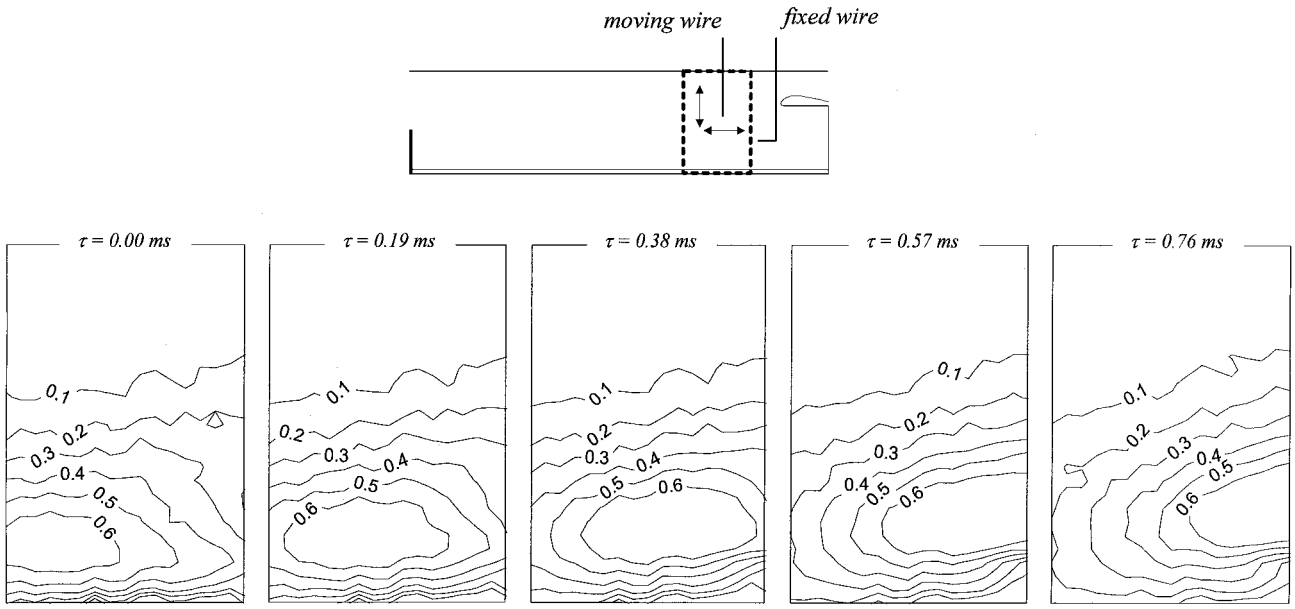

Fig. 13 Map of isocorrelation $R_{uu}(\tau, \delta_x, \delta_y)$ with regard to time delay τ; fixed wire location at ($X = 0.95$, $Y = 0.30$).

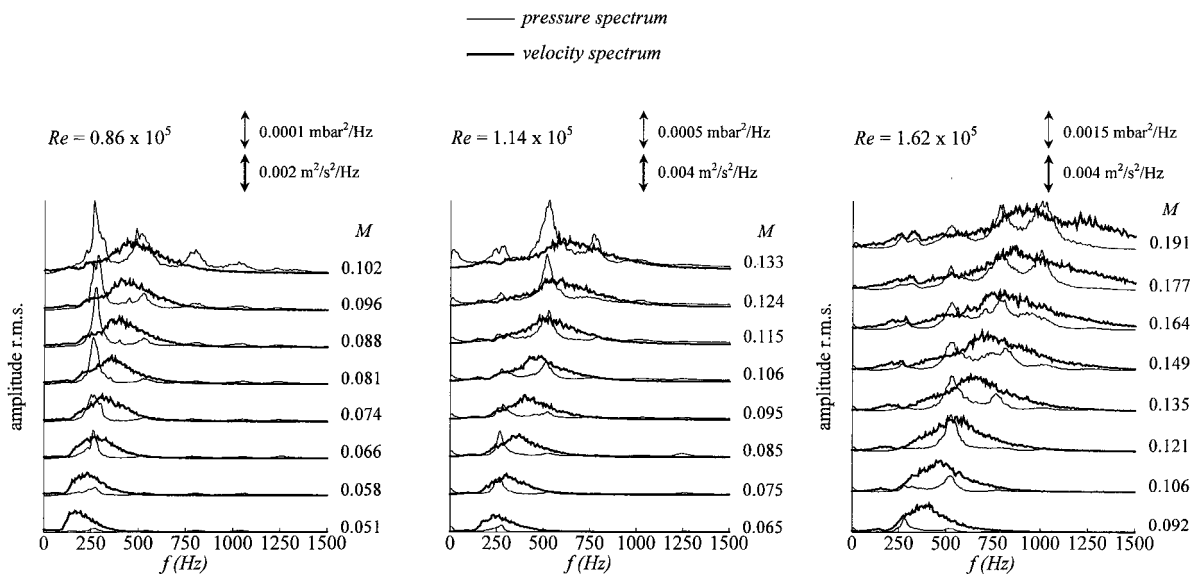

Fig. 14 Spectra comparison of pressure fluctuation at head end and velocity fluctuation at ($X = 0.99$, $Y = 0.10$) at three Reynolds-number levels.

Nevertheless, although vortex-shedding frequency in the obstacle's wake matches up with the first acoustic modes and most excited pressure fluctuation frequency is modified by the flow itself, no direct link was found that could explain why the first four acoustic modes are excited. Indeed, highest turbulence levels are reached close to the injecting walls for $X \geq 0.60$ underlining that instabilities strengthen in this part of the flow. To reach conclusions on the deterministic behavior of turbulence close to the injecting walls, specific measurements were carried out. Space-time correlation coefficient $R_{u_1 u_2}(\tau, \delta_x, \delta_y)$ on velocity fluctuations was estimated by comparing the fluctuating velocity signal at a fixed location ($X = 0.96$, $Y = 0.30$) with the one at a changeable location (Fig. 13). The correlation measurements that result from both δ_x longitudinal and δ_y lateral separation of the velocity probes are also presented in Fig. 13 in the form of an isocorrelation contour map obtained at different time delay τ. As velocity signals were recorded by two single-wire probes, the map can provide only a qualitative description of the fluctuation organization close to the injecting walls. For instance, at $\tau = 0$ ms a large-scale structure is clearly detected with correlation coefficients higher than 60%. The maps at another time delay τ allow as to follow the convection of the large-scale structure with time. Indeed, it is clearly evident that the structure path is slightly shifted up as a result of the blowing effect of the injecting walls. The actual size d in which correlation coefficients are higher than 60% is quite remarkable with d/h_c, close to 0.30 and strongly supports the possibility of a convection structure near the injecting walls. In fact, structure generation near the wall was clearly identified by Brown et al.[15] and Avalon[8] but in a chamber without any geometric disturbance. Furthermore, existence of such structures was demonstrated in wall injection chamber if frequency and acoustical receptivity criteria were respected. Because of our chamber geometry, i.e., as a result of the presence of an obstacle, no credibility can be given to such criteria. For instance, the frequency criterion states that acoustic excitation occurs when an acoustic frequency is higher than a critical hydrodynamic frequency. This frequency can be estimated thanks to the linear stability[23] theory and is reached at a given axial location X_c (Table 1). Considering that X_c must be higher than 1.58 and that the flow reorganizes downstream from the obstacle location, then instabilities observed cannot be caused by linear stability development. In fact, presence of structures in the wake of the obstacle certainly creates a high unstable potential in the flow, and vortices near the injecting walls result from these instabilities. Presence of such vortex structures can be of decisive importance in the unstable behavior of the whole chamber. To evaluate the effect of

such structures, we have compared the spectral response of the characteristic velocity fluctuations at ($X = 0.99, Y = 0.10$), i.e., near the injecting walls with the pressure fluctuations measured at the head end. Indeed, Fig. 14 presents spectral response with regard to Mach number for three Reynolds-number levels. At $Re = 0.86 \times 10^5$ spectral containing in the velocity fluctuations is mainly characterized by a large peak in the neighborhood of f_{1L}. When Mach number increases, this peak is shifted toward higher frequencies and contributes to an energy increase in the thinner pressure spectral peak at f_{1L}. The chamber acts as a resonator. The higher the Mach-number value, the higher the velocity convection of wall structures and then, the higher the characteristic velocity frequency. For $M = 0.106$ as the velocity frequency band is over f_{2L}, the pressure fluctuation energy is amplified at f_{2L}. In fact, it is clearly evident that when the Mach number increases, whatever the Reynolds number is, the characteristic frequency of the "wall vortex" increases and impinges the rear end of the chamber; thus, the chamber naturally excites the neighborhood acoustic frequency. It must be noticed that $R_{u'P'}(\tau)$ reaches a level higher than 50% in the whole range of Mach and Reynolds numbers. This clearly indicates that the noise in the chamber arises essentially from the wall vortex phenomenon. For instance, at $Re = 1.14 \times 10^5$, f_{2L} becomes the higher excited mode because the hydrodynamic conditions near the wall set a large frequency band energy centered at this frequency. The same trend is observed for $Re = 1.62 \times 10^5$. Furthermore, as the hydrodynamic which drives the vortex is mainly a function of the velocity level, the higher Reynolds number, the larger the available velocity range (Table 1) and the higher the excited frequency. This then explains why the first four acoustic modes can be excited with the highest Reynolds number studied when a vortex-shedding phenomenon in the wake of the obstacle takes place at a lower frequency. The selectivity process of the predominant acoustic mode, which coincides with a phenomenon of energy transfer between the various excited modes arises essentially from the hydrodynamic conditions setting the wall vortex frequency.

VI. Conclusions

The coupling phenomenon between acoustics and hydrodynamics was studied in a wall injection chamber in the presence of an obstacle. Experiments were carried out in a wide range of Reynolds-number levels, i.e., in a variable mass flow rate, in order to specify the influence of hydrodynamic conditions on the coupling phenomenon. First of all, it must be underlined that the Mach-number level, whatever the Reynolds number, is a predominant parameter in the flow stability. Coherent structures are generated in the wake of the obstacle thanks to the development of a highly sheared flow. When these structures are sufficiently energetic, they are able to maintain their coherence from the obstacle position to the rear end. Thus, their impingement upon the rear end generates pressure waves, which, by a feedback phenomenon, set the vortex-shedding frequency. This organization was clearly demonstrated by correlation coefficient measurement between pressure and velocity fluctuations. When this coupling occurs, the limited variation in Mach-number levels underlines the constant Strouhal-number evolution of the unstable behavior of the flow. In fact, Reynolds-number influence is mainly characterized by an increase of the available Mach-number range. For the highest Reynolds number studied the shear layer is not organized at the highest excited acoustic mode. Results underline the presence of a pairing phenomenon, which allows for the vortex frequency to match up essentially with f_{1L}. Furthermore, the highest peak at f_{3L} and f_{4L} in the pressure spectral response correspond to the phenomenon of vortex creation near the injecting wall. Present results demonstrate in this kind of chamber the possible coexistence of vortex shedding in the wake of the obstacle and vortex structure generation near the injecting wall. Path convection of such structures follows the latter, and then these structures impinge upon the rear end. This produces noise, which is at the origin of modes transitions. The higher the Mach-number levels, the higher the characteristic frequency of these wall structures and the higher the excited acoustic modes.

A mixing effect has been observed between vortices in the obstacle's wake and structures generated near the injecting wall. Thus, in order to develop stability theory in such chamber, it is necessary to take into account these mixing effects, which generate higher noise levels. Nevertheless, as shown in results, structures created near the injecting wall arise from the interaction of the shear layer downstream from the obstacle and the injecting wall. Finally, when we intend to reduce such noise and to create a more stable state in the whole chamber, impact region can play a significant role. For instance, blowing effect, by lowering or heightening injection velocity, can significantly reduce both vortex generation near the wall and pressure fluctuation energy. On the other hand, impact of injecting walls on turbulence development has not yet been studied even though it could interfere with the vortex-shedding mechanism, i.e., with vortex coherence. Moreover, turbulence in such a flow is complex and occurs with a wide range of characteristic hydrodynamic or acoustic scales. Within the scope of a solid propellant rocket motor study, it may well be necessary to examine whether wall-injected turbulence effects could suffice to avoid the negative consequence of a hydrodynamic-acoustic coupling.

Acknowledgments

This research was sponsored by the Centre National d'Etudes Spatiales (CNES). We give special thanks to Robert Bec, Director of the Solid Propulsion Department, for his tireless aid. These studies were performed within the framework of a research program of the entitled "Aerodynamics of Solid Segmented Motors" of the CNES, concerning the MPS/P230 of Ariane 5, and as a result of a research convention with the Office National d'Etudes et de Recherches Aérospatiales.

References

[1] Mathes, H. B., "Assessment of Chamber Pressure Oscillations in Shuttle Solid Rocket Booster Motor," AIAA Paper 80-1091, June 1980.

[2] Blomshield, F. S., and Mathes, H. B., "Pressure Oscillations in Post-Challenger Space Shuttle Redesigned Solid Rocket Motors," *Journal of Propulsion and Power*, Vol. 9, No. 2, 1993, pp. 217–221.

[3] Scippa, S., Pascal, P., and Zanier, F., "Ariane 5 MPS Chamber Pressure Oscillations Full Scale Firings Results Analysis and Further Studies," AIAA Paper 94-3068, June 1994.

[4] Vuillot, F., "Vortex Shedding Phenomena in Solid Rocket Motors," *Journal of Propulsion and Power*, Vol. 11, No. 4, 1995, pp. 626–639.

[5] Flandro, G. A., "Vortex Driven Mechanism in Oscillatory Rocket Flows," *Journal of Propulsion and Power*, Vol. 2, No. 3, 1986, pp. 206–214.

[6] Dunlap, R., and Brown, R. S., "Exploratory Experiments on Acoustic Oscillations Driven by Periodic Vortex Shedding," *AIAA Journal*, Vol. 19, No. 3, 1981, pp. 408, 409.

[7] Plourde, F., Poisson, R., and Doan-Kim, S., "Space Correlation Measurements in a Forced Shear-Layer with Wall Injection," *Experiments in Fluids*, No. 21, 1996, pp. 26–32.

[8] Avalon, G., "Simulative Study of the Unsteady Flow Inside a Solid Rocket Motor," AIAA Paper 91-1866, June 1991.

[9] Mettenleiter, M., Haile, E., and Candel, S., "Contrôle Actif des Instabilités Aéroacoustiques," *3rd Colloque R&T*, Vol. 1, Centre National d'Etudes Spatiales, 1998, pp. 169–178.

[10] Couton, D., Plourde, F., and Doan-Kim, S., "Cold Gas Simulation of a Solid Propellant Rocket Motor," *AIAA Journal*, Vol. 34, No. 12, 1996, pp. 2514–2522.

[11] Couton, D., Plourde, F., and Doan-Kim, S., "Analysis of Energy Transfer of a Sheared Flow Generated by Wall Injection," *Experiments in Fluids*, Vol. 26, 1999, pp. 222–232.

[12] Beddini, A. R., "Analysis of Injection Induced Flows in Porous Walled Duct with Application to Aerochemistry of Solid Propellant Motor," Ph.D. Dissertation, Graduate Program in Mechanical and Aerospace Engineering, Rutgers Univ., New Brunswick, NJ, Oct. 1981.

[13] Plourde, F., Couton, D., and Doan Kim, S., "Image Processing for Vortex Visualization and Characterization," *Proceedings of the 8th International Symposium on Flow Visualization*, Vol. 1, Sorrento, Italy, 1998, pp. 363–369.

[14] Flandro, G. A., and Jacobs, H. R., "Vortex Generated Sound in Cavities," AIAA Paper 73-1014, Oct. 1973.

[15] Brown, R. S., Dunlap, R., Young, S. W., and Waugh, R. C., "Vortex Shedding as a Source of Acoustic Energy in Segmented Solid Rockets," *Journal of Spacecraft and Rockets*, Vol. 18, No. 4, 1981, pp. 312–319.

[16] Vetel, J., Plourde, F., and Doan Kim, S., "Influence of Hydrodynamic Conditions on the Vortex Shedding Phenomenon," AIAA Paper 2000-2000, June 2000.

[17] Ho, C. M., and Nosseir, N. S., "Dynamics of an Impinging Jet. Part 1: The Feedback Phenomenon," *Journal of Fluid Mechanics*, Vol. 105, 1981, pp. 119–142.

[18]Rockwell, D., "Oscillations of Impinging Shear Layers," *AIAA Journal*, Vol. 21, No. 5, 1983, pp. 645–664.

[19]Schachenmann, A., and Rockwel, D., "Self-Sustained Oscillations of Turbulent Pipe Flow Terminated by an Axisymmetric Cavity," *Journal of Sound Vibration*, Vol. 73, No. 1, 1980, pp. 61–72.

[20]Rockwell, D., and Naudasher, E., "Self-Sustained Oscillations of Impinging Free Shear Layers," *Annual Review of Fluid Mechanics*, Vol. 11, 1979, pp. 67–94.

[21]Lau, J. C., Fisher, M. J., and Fuchs, H. V., "The Intrinsic Structure of Turbulents Jets." *Journal of Sound and Vibration*, Vol. 22, 1972, pp. 379–406.

[22]Neuwerth, G., "Akustiche Ruckkopplungserscheinungenam Unter-und Uberschall-Freistrahl, der auf einen Storkorper Trifft," Dr. Ing. Thesis, Tech. Hoschs Aachen, Aachen, Germany, 1973.

[23]Avalon, G., Casalis, G., and Griffond, J., "Flow Instabilities and Acoustic Resonance of Channels with Wall Injection," AIAA Paper 98-3218, July 1998.

[24]Soreefan, S., "Contribution à l'Etude des Bruits Auto-Entretenus Crées par un Jet Confiné Rencontrant un Obstacle," Ph.D. Dissertation, Univ. of Poitiers, Poitiers, France, Oct. 1993.

[25]Flatau, A., "Vortex Driven Sound in a Cylindrical Cavity," Ph.D. Dissertation, Univ. of Utah, Salt Lake City, UT, Oct. 1990.

[26]Jones, J. H., Guest, S. H., Matienzo, J. J., and Reed, D. K., "Acoustic Overpressure and Unsteady Flow Phenomena Associated with the Saturn/Space Shuttle Systems: A Review of Selected Issues," *Colloque International Ambiance Acoustique et Vibratoire des Systèmes de Transport Spatial*, Jouy-en-Josas, France, Feb. 1994.

J. P. Gore
Associate Editor